Missouri University of Science and Technology
Scholars' Mine

Mechanical and Aerospace Engineering Faculty Research & Creative Works

Mechanical and Aerospace Engineering

01 May 2017

Infrared Metasurfaces Created with Off-Normal Incidence Microsphere Photolithography

Chuang Qu

Edward C. Kinzel
Missouri University of Science and Technology, kinzele@mst.edu

Follow this and additional works at: https://scholarsmine.mst.edu/mec_aereng_facwork

Part of the Mechanical Engineering Commons

Recommended Citation

C. Qu and E. C. Kinzel, "Infrared Metasurfaces Created with Off-Normal Incidence Microsphere Photolithography," *Optics Express*, vol. 25, no. 11, pp. 12632-12639, Optical Society of America (OSA), May 2017.
The definitive version is available at https://doi.org/10.1364/OE.25.012632

This Article - Journal is brought to you for free and open access by Scholars' Mine. It has been accepted for inclusion in Mechanical and Aerospace Engineering Faculty Research & Creative Works by an authorized administrator of Scholars' Mine. This work is protected by U. S. Copyright Law. Unauthorized use including reproduction for redistribution requires the permission of the copyright holder. For more information, please contact scholarsmine@mst.edu.

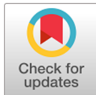

Research Article Vol. 25, No. 11 | 29 May 2017 | OPTICS EXPRESS 12632

Optics EXPRESS

Infrared metasurfaces created with off-normal incidence microsphere photolithography

CHUANG QU AND EDWARD C. KINZEL*

Department of Mechanical and Aerospace Engineering, Missouri University of Science and Technology, 400 West 13th Street, Rolla, MO 65409, USA

*kinzele@mst.edu

Abstract: Fabricating metasurfaces over large areas at low costs remains a critical challenge to their practical implementation. This paper reports on the use of microsphere photolithography (MPL) to create infrared metasurfaces by changing the angle-of-incidence of the illumination to steer the photonic jet. The displacement of the photonic jet is shown to scale with the diameter of the microsphere while the exposure dose scales with the square of the microsphere diameter. This process is robust in the presence of local defects in the microsphere lattice. The paper demonstrates patterning split ring resonators and tripole based metasurfaces using MPL, which are fabricated and characterized with FTIR. The combination of bottom-up and top-down approaches in off-normal incidence microsphere photolithography technique provides cost-effective, flexible, and high-throughput fabrication of infrared metasurfaces.

© 2017 Optical Society of America

OCIS codes: (110.4235) Nanolithography; (160.3918) Metamaterials; (220.4241) Nanostructure fabrication; (310.6628) Subwavelength structures, nanostructures.

References and links

1. J. B. Pendry, "Negative refraction makes a perfect lens," Phys. Rev. Lett. **85**(18), 3966–3969 (2000).
2. L. Wang, S. Kruk, H. Tang, T. Li, I. Kravchenko, D. N. Neshev, and Y. S. Kivshar, "Grayscale transparent metasurface holograms," Optica **3**(12), 1504–1505 (2016).
3. X. Ni, Z. J. Wong, M. Mrejen, Y. Wang, and X. Zhang, "An ultrathin invisibility skin cloak for visible light," Science **349**(6254), 1310–1314 (2015).
4. C. Qu and E. C. Kinzel, "Polycrystalline metasurface perfect absorbers fabricated using microsphere photolithography," Opt. Lett. **41**(15), 3399–3402 (2016).
5. B. Lahiri, A. Z. Khokhar, R. M. De La Rue, S. G. McMeekin, and N. P. Johnson, "Asymmetric split ring resonators for optical sensing of organic materials," Opt. Express **17**(2), 1107–1115 (2009).
6. Y. Zhang, L. Zhou, J. Q. Li, Q. J. Wang, and C. P. Huang, "Ultra-broadband and strongly enhanced diffraction with metasurfaces," Sci. Rep. **5**(1), 10119 (2015).
7. J. A. D'Archangel, D. J. Shelton, R. Hudgins, M. K. Poutous, and G. D. Boreman, "Large area infrared frequency selective surface with dimensions reproducible by optical lithography," J. Vac. Sci. Technol. B **32**(5), 051807 (2014).
8. L. J. Guo, "Nanoimprint lithography: methods and material requirements," Adv. Mater. **19**(4), 495–513 (2007).
9. I. B. Divliansky, A. Shishido, I.-C. Khoo, T. S. Mayer, D. Pena, S. Nishimura, C. D. Keating, and T. E. Mallouk, "Fabrication of two-dimensional photonic crystals using interference lithography and electrodeposition of CdSe," Appl. Phys. Lett. **79**(21), 3392–3394 (2001).
10. J. C. Hulteen and R. P. Van Duyne, "Nanosphere lithography: a materials general fabrication process for periodic particle array surfaces," J. Vac. Sci. Technol. A **13**(3), 1553–1558 (1995).
11. M. C. Gwinner, E. Koroknay, L. Fu, P. Patoka, W. Kandulski, M. Giersig, and H. Giessen, "Periodic Large-Area Metallic Split-Ring Resonator Metamaterial Fabrication Based on Shadow Nanosphere Lithography," Small **5**(3), 400–406 (2009).
12. W. Wu, D. Dey, O. G. Memis, A. Katsnelson, and H. Mohseni, "Fabrication of large area periodic nanostructures using nanosphere photolithography," Nanoscale Res. Lett. **3**(10), 351–354 (2008).
13. Z. Szabó, J. Volk, E. Fulop, A. Deak, and I. Barsony, "Regular ZnO nanopillar arrays by nanosphere photolithography," Phot. Nano. Fund. Appl. **11**(1), 1–7 (2013).
14. Y. C. Chang, S. M. Wang, H. C. Chung, C. B. Tseng, and S. H. Chang, "Observation of absorption-dominated bonding dark plasmon mode from metal-insulator-metal nanodisk arrays fabricated by nanospherical-lens lithography," ACS Nano **6**(4), 3390–3396 (2012).
15. X. Li, Z. Chen, A. Taflove, and V. Backman, "Optical analysis of nanoparticles via enhanced backscattering facilitated by 3-D photonic nanojets," Opt. Express **13**(2), 526–533 (2005).

#286885 https://doi.org/10.1364/OE.25.012632
Journal © 2017 Received 16 Feb 2017; revised 1 May 2017; accepted 10 May 2017; published 22 May 2017

Optics EXPRESS

16. M. S. Kim, T. Scharf, S. Mühlig, M. Fruhnert, C. Rockstuhl, R. Bitterli, W. Noell, R. Voelkel, and H. P. Herzig, "Refraction limit of miniaturized optical systems: a ball-lens example," Opt. Express **24**(7), 6996–7005 (2016).
17. M. H. Wu, C. Park, and G. M. Whitesides, "Generation of submicrometer structures by photolithography using arrays of spherical microlenses," J. Colloid Interface Sci. **265**(2), 304–309 (2003).
18. A. Bonakdar, S. J. Jang, and H. Mohseni, "Novel high-throughput and maskless photolithography to fabricate plasmonic molecules," J. Vac. Sci. Technol. B **32**(2), 020604 (2014).
19. Y. Zhang, T. Wei, Z. Xiong, L. Shang, Y. Tian, Y. Zhao, P. Zhou, J. Wang, and J. Li, "Enhanced optical power of GaN-based light-emitting diode with compound photonic crystals by multiple-exposure nanosphere-lens lithography," Appl. Phys. Lett. **105**(1), 013108 (2014).
20. A. Bonakdar, M. Rezaei, R. L. Brown, V. Fathipour, E. Dexheimer, S. J. Jang, and H. Mohseni, "Deep-UV microsphere projection lithography," Opt. Lett. **40**(11), 2537–2540 (2015).
21. W. Guo, Z. B. Wang, L. Li, D. J. Whitehead, B. S. Luk'yanchuk, and Z. Liu, "Near-field laser parallel nanofabrication of arbitrary-shaped patterns," Appl. Phys. Lett. **90**(24), 243101 (2007).
22. X. Meng and D. Qiu, "Gas-flow-induced reorientation to centimeter-sized two-dimensional colloidal single crystal of polystyrene particle," Langmuir **30**(11), 3019–3023 (2014).
23. D. J. Shelton, I. Brener, J. C. Ginn, M. B. Sinclair, D. W. Peters, K. R. Coffey, and G. D. Boreman, "Strong coupling between nanoscale metamaterials and phonons," Nano Lett. **11**(5), 2104–2108 (2011).
24. B. A. Munk, *Frequency Selective Surfaces Theory and Design* (John Wiley & Sons, 2000).
25. J. Ginn, D. Shelton, P. Krenz, B. Lail, and G. Boreman, "Polarized infrared emission using frequency selective surfaces," Opt. Express **18**(5), 4557–4563 (2010).

Metasurfaces and Frequency Selective Surfaces (FSS) are composite structures that provide an engineered electromagnetic scattering response. They consist of subwavelength antenna elements whose 2D geometry determines the ensemble properties. These surfaces have applications such as planar lenses [1], holograms [2], carpet cloaks [3], perfect absorbers [4], Surface-Enhanced Raman Spectroscopy (SERS) and Surface-Enhanced Infrared Absorption (SEIRA) templates [5]. The subwavelength nature of these devices requires nanoscale patterning at infrared and optical frequencies. Metasurfaces can be readily prototyped using direct-write techniques such as Electron-Beam Lithography (EBL) [2,5] or Focused Ion Beam (FIB) milling [6], however, these techniques are cost prohibitive for practical applications where the nanoscale features in the metasurface must be patterned over cm^2 to m^2 areas. The inability to fabricate metasurfaces over these length scales is the principal obstacle to the implementation of metasurfaces to practical engineering problems.

Conventional projection lithography is possible for IR/THz FSS with µm + feature sizes and has been demonstrated for patch type perfect absorbers in the MWIR [7]. However, this becomes very expensive on an area basis for more complicated nanoscale features due to the requirements for masks and steppers. Similar cost/reliability concerns exist for developing variants of Nanoimprint Lithography [8] when it is applied at large scales. Interference lithography can also create arrays of patches/disks [9] but requires precise alignment and is limited for creating sub-element nanoscale features. Another option is colloidal techniques based on the self-assembly of microspheres into a Hexagonal Close Packed (HCP) lattice. This includes Nanosphere Lithography (NSL) [10] where the microsphere array is used as a shadow mask during PVD evaporation or etching. The NSL technique can be used to create complicated patterns including functional IR resonators using directional evaporation [11]. However, in NSL the microspheres are consumed in the process and the technique requires precise manipulation of the sample in high-vacuum. A different approach is to use the self-assembled microspheres as optical elements to focus light. This has been termed microsphere/nanosphere photolithography (MPL/NPL) [12,13], and Nanoparticle Lens Lithography (NLL) [14]. In this technique, the microspheres are in contact with a photoresist layer and produce and focus incident light to a photonic jet [15] with FWHM width of $\lambda/3$. This is a result of both evanescent and propagating fields which allows the subwavelength photonic jet to extend more than λ into the photoresist [16]. The MPL technique has previously been used for pattering metasurfaces/FSS [4, 13]. The resonator size and hence wavelength was shown to be dependent on the illumination dose providing a pathway to hierarchical patterning of metasurfaces. This differs slightly from the Microlens Projection Lithography approach developed by the Whitesides group [17] where the microspheres,

embedded in an elastomeric membrane, are separated from the photoresist and used to image a far-field pattern onto the photoresist.

Mohseni et al. demonstrated steering the photonic jet around the unit cell by tilting the substrate under collimated radiation [18,19] or by controlling the angular spectrum of the illumination using a Fourier mask [20]. Using Deep UV (248 nm) illumination, they were able to define sub 100 nm features [20], included the creation of both holes and posts using positive and negative tone resists, respectively. This approach was also used by Zhang et al. [19] to fabricate nanostructures for enhancing the emission from LEDs and previously by Guo et al. [21] for the ablation of 360 nm wide lines in a thin SbTe film using silica microspheres and off normal illumination using a KrF excimer laser.

The objective of this paper is to explore the off-normal incidence MPL pattering process for the fabrication of IR metasurfaces. The process is introduced and characterized with respect to both the exposure of the photoresist as well as lift-off. The microsphere size, exposure dosage and incident angle are mapped experimentally and through simulation. Finally, functional infrared metasurfaces featuring split-ring resonators and tripoles are fabricated using the technique. These metasurfaces are also characterized experimentally and compared to simulation. The results demonstrate the robustness of the process with respect to local disorder in the microsphere lattice and show ability to pattern a wide range of practical metasurfaces.

Figure 1 illustrates the general fabrication process for microsphere photolithography. The microspheres are self-assembled onto a photoresist film, forming a Hexagonal Close-Packed (HCP) lattice. Several different techniques have been developed for self-assembling the microspheres [22] including convective self-assembly and liquid interface assembly. After the spheres are self-assembled and any excess solvent is removed, the microspheres are illuminated with UV light at angle measured from the surface normal (θ, φ) shown in Fig. 1(a). Each microsphere focuses the incident light to a photonic jet inside the photoresist layer. The development process removes the spheres as well as the photoresist from the exposed regions to reveal the desired pattern as shown in Fig. 1(b). Patterns can be transferred to the substrate using standard techniques such as etching or lift-off. Lift-off is used in this paper to deposit metal patterns (Fig. 1(c)).

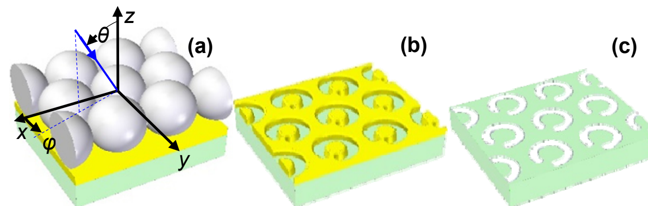

Fig. 1. Illustration of fabrication procedure (a) directional illumination of self-assembled microspheres from polar angle, θ, and azimuthal angle, φ, (b) pattern revealed in photoresist after exposure and development (c) final metal split-ring resonators after lift-off.

Figure 2 shows results of frequency-domain finite element method simulation (ANSYS HFSS) of the off-axis exposure process. A Floquet modal expansion is used to model an infinitely periodic hexagonal close packed array of polystyrene (n = 1.69) microspheres rests on a 480 nm thick layer of S1805 (n = 1.73) which is on top of a BK7 glass (n = 1.52) substrate. The microspheres are illuminated with a λ_0 = 365 nm (i-line) plane wave at φ = 0. Figures 2(a-c) shows the normalized electric field energy distribution under θ = 20° for different sized microspheres on the xz plane as well as the midplane of the photoresist (z = −240 nm). In each case, the incident field is collected by the sphere and focused to a confined jet with FWHM ~λ_0/3. The normalized electric field energy is plotted in Fig. 2(d) for p = 3 μm spheres at the surface, midplane, and substrate interface of the photoresist (z = 0, −240, and −480 nm) under different angles of illumination. The intensity of the jet

Optics EXPRESS

scales with ~p^2 (the cross sectional capture area of the spheres). The FWHM diameter increases with the angle of incidence. The center of the photonic jet is offset from the center of the microsphere by a displacement, δ, which scales with θ. This relationship can be normalized with the sphere diameter so that δ/p is constant for a given θ. This displacement is almost independent of φ. The simulations agree with a first order paraxial model for the process where the focus of the microsphere shifts with angle of incidence $\delta = f{\cdot}\theta$, where the focal length f of a ball lens in air is given by $f = n{\cdot}p/[4(n\text{-}1)]$.

A set of two-step illumination experiment was performed to verify the simulation results. Microposit S1805 positive tone photoresist was spun to a thickness of 480 nm on a glass microscope slide. After softbaking of the photoresist, polystyrene microspheres (Polysciences, Inc.) are drop-coated (convective self-assembly) onto the photoresist film. The illumination angles are determined by two computer controlled rotation stages positioned under a stationary *i*-line flood exposure source (Bachur). The stages enable continuous rotation of the polar angle $-90°<\theta<90°$ and azimuthal angle $0\leq\varphi<360°$. For this experiment, the samples were exposed at polar angle θ, rotated to angle $-\theta$, and exposed a second time. After the exposures, the samples are immersed in MF 319 developer (Dow), followed by rinsing with deionized water and drying with compressed air, before hard baking. This generates two holes centered around the center of the microsphere.

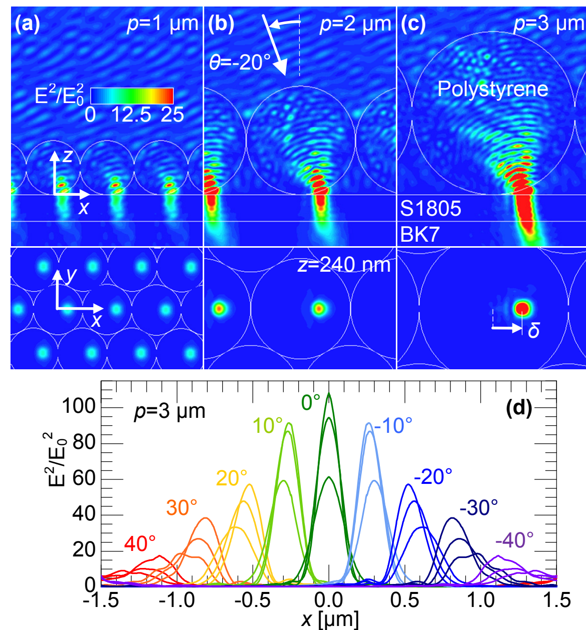

Fig. 2. Simulation of off-axis exposure of different sized microspheres. Normalized electric field energy distribution (a) 1 µm (b) 2 µm and (c) 3 µm for −20° off normal illumination and (d) response at 0, 240 and 480 nm depths into the photoresist under different angles of incidence for 3 µm microspheres.

Figure 3 shows SEM images of different hole-pairs generated with p = 3 µm spheres. The photoresist was cross sectioned using FIB milling (Helios Nanolab 600, FEI) through the center of each hole pair. Figure 3(a) shows partially exposed holes generated with two-step illumination at $\theta = \pm$ 10° at a dose of 1.44 mJ/cm^2 each time. The holes are separated by 2δ = 670 nm and do not completely penetrate the photoresist (diameter ~220 nm in diameter). Figure 3(b) shows the results of illuminating a different sample by $\theta = \pm$ 10° but with an increased dose of 3.6 mJ/cm^2. The center-to-center separation is the same but the exposed holes clear the photoresist with a diameter of 520 nm. When the illumination angle is increased to 25° off normal, the separation increases to 2δ = 1530 nm, and the diameter of the

holes increases to 700 nm as shown in Fig. 3(c). The increase in the hole diameter with larger angles of incidence agrees with the predictions of simulation shown in Fig. 2(d).

Evaporation and lift off were performed to study the effects of the exposure angle in a pattern transfer scenario. A 100 nm-thick aluminum film was deposited onto the patterned photoresist. The photoresist was then stripped using ultrasonication and Remover PG (MicroChem) to reveal metallic micro/nano features on the substrate. The convective self-assembly procedure (drop-coating) creates polycrystalline arrays of microspheres with grains in different orientations. As a result, the azimuthal angle varies from grain to grain. Figure 4 shows disk pairs in different orientations. The disks are equidistant from the center of the spheres and their position depends on the location of the spheres and polar angle but is independent of the azimuthal angle. This agrees with simulation and allows the creation of detailed patterns without needing to align the crystal orientation to the illumination.

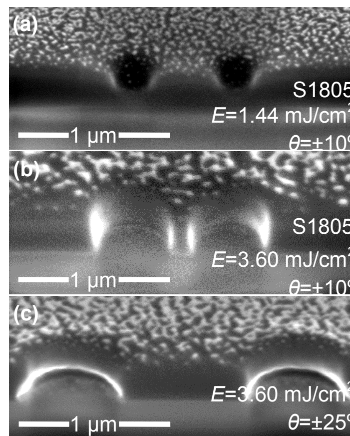

Fig. 3. SEM images taken from 52° of hole-pairs after FIB cross sectioning (a) 1.44 mJ/cm^2, ± 10°; (b) 3.6 mJ/cm^2, ± 10°; (c) 3.6 mJ/cm^2, ± 25°. Au/Pd was sputtered onto the photoresist prior to imaging to avoid charging.

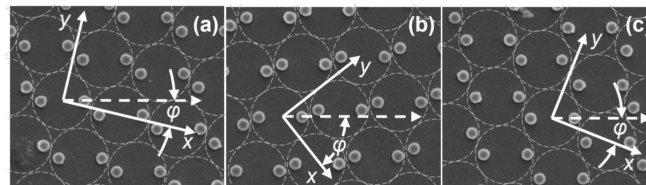

Fig. 4. (a)-(c) SEM images of disks pairs (E = 7.2 mJ/cm2, θ = ± 35°, p = 3 μm) after lift-off (a) φ = 13°, (b) φ = 52°, and (c) φ = 22° resulting from different orientations of the microsphere lattice relative to the illumination directions.

Figure 5 plots the measured displacement, δ, of the disk pairs from the center of the microspheres produced with illumination from different polar angles. Both p = 2 and 3 μm microspheres were used and the displacement scales linearly with the microsphere diameter and the illumination angle. The dose affects the size of the disk but does not change the offset. The error bars in the figure represent the variation in the separation over a 100 μm × 100 μm area. In this experiment angles less than θ = 10° resulted in the disks merging together. The dashed lines in Fig. 5 show the center of the photonic jet predicted by the HFSS simulation (Fig. 2) at the top surface of the photoresist and the photoresist/glass interface.

Figures 4 and 5 show the robustness of the MPL process. Structures will take on the HCP lattice of the microsphere array including the microstructure resulting from the self-assembly

Optics EXPRESS

process. The spherical coordinates of the illumination system map to polar coordinates in the unit cell; the azimuthal angle does not change and the polar angle determines the radial displacement with a nearly linear mapping between $\theta = 0$ and 45° corresponding to the center and edge of the unit cell. The feature size scales with the exposure dose [4].

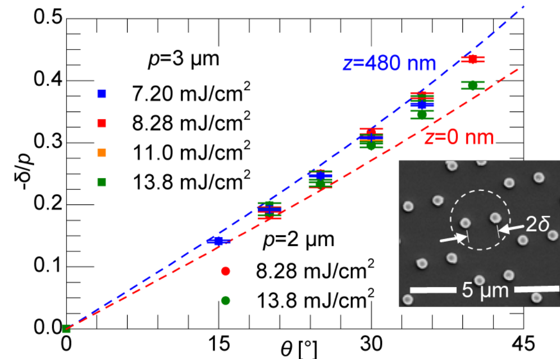

Fig. 5. Measured disk displacement normalized to sphere diameter for deposited disks produced with different incident angles. Dashed lines show simulated displacement at the top and bottom of the photoresist.

IR metasurfaces can be designed for these constraints. To explore this, we used the technique to pattern two different functional devices. Figure 6 shows results from an array of Split Ring Resonators (SRR). These are a widely studied metamaterial element because of the ability of the SRR to create an artificial magnetic response as well as sensing applications. The fundamental resonance has a half-wave current response in the bent wire elements providing an inductive response. The electric field is concentrated in the gap region which enhances the capacitance. This leads to a dipole response parallel to the gap, so that the fundamental resonance will be excited when the incident E-field is polarized across the gap.

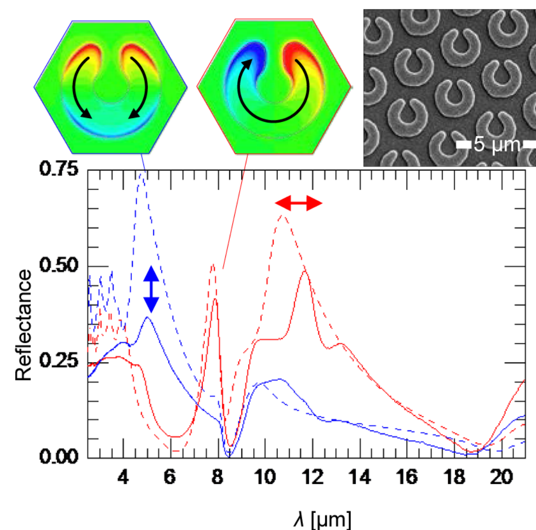

Fig. 6. Reflectance spectra of split ring resonator sample shown in the SEM image. Red and blue lines represent the response for incident radiation polarized parallel and perpendicular to the SRR gap. The solid and dashed lines show FTIR and simulation results, respectively. Field distributions (normal component of E-field at λ = 4.8 and 7.8 μm) are shown for the two primary resonances.

The SRRs in Fig. 6 were created by spin-coating 480 nm of S1805 onto a glass microscope slide. Microspheres, p = 3 μm, were drop-coated onto the photoresist. This leads to cm^2 areas with single crystals on the order of 300 μm. The microsphere array was illuminated from θ = 30°. From Fig. 5, this corresponds to a diameter of 1.8 μm (2δ). A second computer controlled stage was use to rotate φ from 0 to 345° in $\Delta\varphi$ = 15° steps. At each step the sample was exposed using a fluence of E = 7.2 mJ/cm^2. After development and hardbaking, lift-off was used to transfer 100 nm thick aluminum patterns to the substrate. The width of the features shown in the inset of Fig. 6 is 750 nm. The dimensions of the SRR were selected to place the primary resonant mode at the same wavelength silica absorption peak due to phonon mode coupling [23].

The reflectance spectra of the metasurface were measured using Fourier Transform Infrared (FTIR) spectrometer (Perkin-Elmer micro-FTIR). The SRRs have a distinct linearly polarized response which is dependent by the orientation of the gap. The gap's angular position is determined in the specimen rather than the lattice coordinate system. Figure 6 shows the measured reflectance of the SRRs for radiation polarized parallel to the gap in red and the perpendicular to the gap in blue. The dashed lines show the simulated response of the metasurface from HFSS. In the simulation, the glass microscope slide is modeled as SiO_2. The properties of both SiO_2 and Al are taken from IR ellipsometry. The insets show simulated normal E-field distributions at the surface of the SRR for the three lowest energy modes (λ = 7.8, 4.7, and 3.8 μm) with arrows indicating the direction of current flow. There is reasonable agreement between the experimental and simulated reflectance spectra, with the discrepancy attributable to uncertainty in the substrate dielectric properties.

Figure 7 shows results for a Metal-Insulator-Metal tripole based metasurface absorber/emitter patterned with MPL. A tripole is a common Frequency-Selective Surface (FSS) element used at microwave frequencies [24] and is polarization independent because the two orthogonal modes share common current paths [25]. The presence of the ground plane prevents any transmission, so that radiation not reflected by the surface is absorbed. From Kirchhoff's law the absorptance is equal to the emittance, so the device acts as a selective emitter with applications for controlling thermal transport. The tripoles are separated from a 200 nm thick aluminum ground plane by a 250 nm silicon dioxide film. As with the SRRs, 3 μm microspheres were used. The sample was exposed at θ = 15°, 20°, and 25° at three different relative azimuthal angles, φ = 0°, 120° and 240° (9 steps) with a fluence of E = 7.2 mJ/cm^2. Figure 7 shows agreement between the unpolarized reflectance measured with FTIR and HFSS simulation.

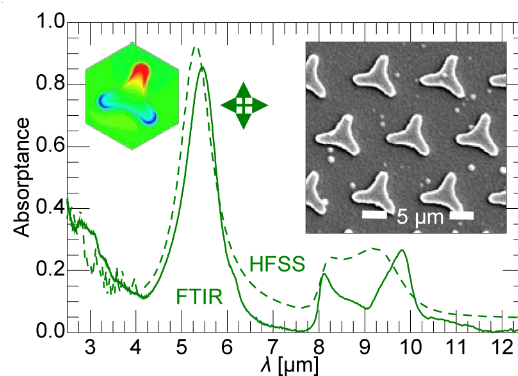

Fig. 7. Absorption spectra of tripole FSS shown in the inset (SEM image). The solid and dashed lines show FTIR and simulation results, respectively.

The tripoles show a single resonance at λ = 5.5 μm with an absorptance greater than 0.85. This can be tuned by adjusting the illumination angles to increase or decrease the tripole arm

Optics EXPRESS

length. The exposure can also be adjusted to control the width of the patterns. There is relatively little coupling between adjacent tripoles so they are also not affected by the lattice orientation. It is important to note that the photonic jet was not significantly affected by the presence of the ground plane, expanding the range of devices that can be patterned with this method.

In conclusion, microsphere photolithography is shown to be a versatile tool for patterning IR metasurfaces. The combination of bottom-up self-assembly of microsphere array and top-down, direct-write exposure allows inexpensive patterning of detailed elements over large areas at low-cost. Control of the illumination angle-of-incidence allows the photonic jet to be precisely steered around the unit cell defined by the microsphere. The displacement of the photonic jet from the center of the microsphere is shown to be independent of the orientation of the microsphere lattice and scales with the microsphere diameter. The width of the exposed region scales with the exposure dose and can be further reduced to facilitate patterning metasurfaces for SWIR or visible wavelengths. The ability to pattern structures with a ground-plane is significant for expanding the types of metasurfaces that can be patterned with the technique and opens more possibilities for spectral engineering and field concentration for sensing applications. Finally, the agreement between idealized simulations of infinitely periodic structures with experimental results for both the MPL process and the metasurfaces illustrates the robustness of the process in the presence of lattice defects and other irregularities from the self-assembly process.

Funding

National Science Foundation (NSF ECCS-1509589); Missouri University of Science and Technology Materials Research Center.

131.151.26.127 {ts '2019-01-09 11:12:53'}